Sensors & Transducers, Vol. 230, Issue 2, February 2019, pp. 14-20

www.sensorsportal.com

Sensors & Transducers

Published by IFSA Publishing, S. L., 2019
http://www.sensorsportal.com

The Automated Lung Segmentation and Tumor Extraction Algorithm for PET/CT Images

[1] Su Yang, [2] Hae Won Kim and [1] Jong-Ha Lee

[1] Department of Biomedical Engineering, Keimyung University, School of Medicine, South Korea
[2] Department of Nuclear Medicine, Keimyung University, School of Medicine, South Korea
[1] Tel.: (82)-53-580-3736, fax: (82)-53-580-3746
E-mail: segeberg@kmu.ac.kr

Received: 30 November 2018 /Accepted: 31 January 2019 /Published: 28 February 2019

Abstract: ^{18}F-fluorodeoxyglucose integrated positron emission tomography and computed tomography (PET/CT) have been extensively used for evaluation of lung tumor. Traditional lung segmentation algorithm have not considered the detection of juxta-pleural nodules or large mass sufficiently and have segmented lung inaccurately. In this study, we developed a novel fully automated lung segmentation and lung tumor extraction algorithm for ^{18}F-FDG PET/CT images in patients with lung cancer. The algorithm consisted of initial lung segmentation, adaptive maximum intensity projection, tumor extraction, and optimal lung segmentation. The validation of the algorithm was accomplished by comparing automated analysis results to the manual analysis results. The dice similarity coefficient, Jaccard index and accuracy of lung segmentation performance were 98.2 %, 96.6 % and 99 %, respectively. In extraction of lung tumor, sensitivity, specificity and accuracy were 87.9 %, 89.9 % and 88.5 %. Our automated algorithm for ^{18}F-FDG PET/CT images performed lung segmentation and lung tumor extraction effectively in patients with lung cancer.

Keywords: Lung segmentation, Lung tumor extraction, Adaptive maximum intensity projection, Seed-based region growing.

1. Introduction

Lung cancer deaths constitute the largest portion of all deaths in Korea and have been further increasing year by year [1]. Mortality from lung cancer is one of the highest mortality rates among cancer related death [2]. The cure rate for lung cancer is relatively high if it is detected early and surgery is performed, and therefore early detection of lung cancer is crucial.

Non-invasive diagnostic imaging tests commonly used for diagnosis of lung cancer include computed tomography (CT) and positron emission tomography (PET). In particular, the diagnostic yield of cancer has been greatly improved since the introduction of PET/CT scanner, which combines CT and PET scanners to provide the body's anatomic and metabolic information [3-5]. With increased amount of PET/CT imaging, however, imaging analysis workload for physicians is growing and cases of nondetection, misdetection, and misinterpretation are increasing. To address these problems, computer aided detection (CADe) and computer aided diagnosis (CADx) technologies may be used. CADe and CADx technologies not only reduce image interpretation time but also enhance consistency of analysis and aid doctors make the final diagnosis through quantitative analysis results. In recent years, studies of CADe and CADx technologies, with the aim to assist doctors interpret images and make decisions, are continuously being reported [6-8].

However, CADe and CADx technologies developed up to now had inaccuracy issues, and interpretation results varied depending on the physician's condition or proficiency in many cases [9]. In addition, CADe and CADx showed limitations in detecting juxtapleural or relatively large lung tumors [10]. Thus, our study aimed to develop a fully automated lung segmentation and lung tumor extraction algorithm for ^{18}F-FDG PET/CT images.

2. Materials and Methods

2.1. Patients

Twenty patients who underwent ^{18}F-FDG PET/CT for staging prior to surgery at our institution were retrospectively reviewed. Patients with history of cancer (other than lung cancer), anatomical abnormalities of the chest, pneumonectomy, or pulmonary inflammatory lesion, as well as patients who underwent lung surgery or received radiotherapy or cancer therapy prior to PEC/CT scan were excluded from the study. This study was approved by the institutional review board of our institution.

2.2. PET/CT Image

All patients fasted for at least six hours, were adequately hydrated (approximately 1 L), and normal blood glucose levels (less than 180 mg/dL) were confirmed before undergoing PET/CT (Biograph mCT-64, Siemens Healthcare, Knoxville, TN) imaging. Sixty minutes after intravenous administration of ^{18}F-FDG (4.0 MBq per kg), CT transmission scan was acquired first, followed by PET emission scan with acquisition time of 2 minutes per bed position. The PET images were reconstructed using the OSEM algorithm (4 iterations, 8 subsets) and corrected for attenuation using the CT images. PET/CT images at five to six bed positions covering the area from the base of the cranium to femoral middle of the thigh were acquired. The CT and PET images used had the same slice thickness and resolutions of 512×512 and 128×128, respectively.

PET/CT images were interpreted independently by two experienced nuclear medicine physicians and the results with consensus reading of the two physicians were analyzed. The results of a fully automated lung tumor extraction algorithm were compared with the manually identified positions of the lung tumors by the nuclear medicine physicians.

2.3. Image Preprocessing Steps

When reconstructing CT images, the intensity value of the void space in an image is not 0 and creates noise, and the table supporting the patient is present in the image. The noises are processed as 0 intensity by thresholding and the thin table supporting the patients is removed using the predefined location data of the table. The Fig 1 shows the diagram.

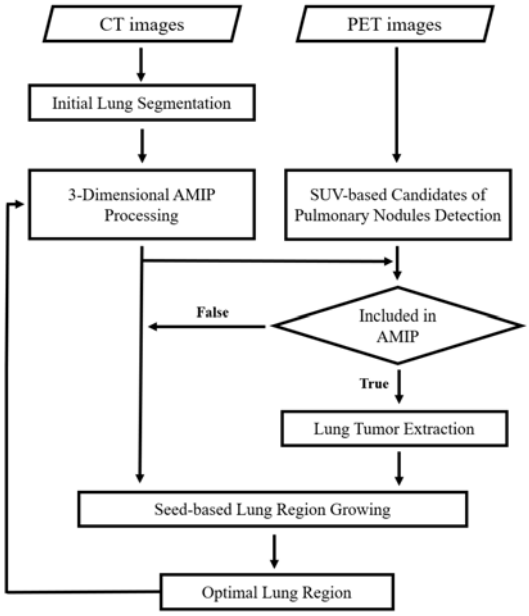


Fig. 1. Diagram of entire process. CT, computed tomography; PET, positron emission tomography; AMIP, adaptive maximum intensity projection; SUV, standardized uptake value.

2.4. Threshold-based Initial Lung Segmentation

For initial lung segmentation, a median filter size of 5 was applied, and then pixels were assigned a binary value using the Otsu algorithm with the threshold value of 0.2 (Fig. 2).

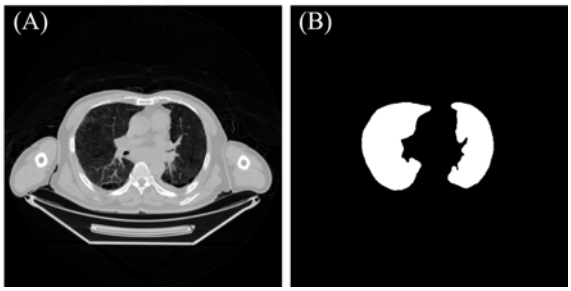


Fig. 2. The threshold-based lung segmentation. (A) Original the computed tomography image, (B) result of initial lung segmentation.

The constructed binary image of initial lung segmentation was used to calculate the adaptive maximum intensity projection (AMIP) and define initial seed points for the seed-based region growing algorithm, which is used for optimal lung segmentation.

2.5. Adaptive Maximum Intensity Projection

In ^{18}F-FDG PET images, high standardized uptake values (SUV) are observed in not only lung tumors but also other organs. In this study, we devised an adaptive maximum intensity projection (AMIP) technique in order to accurately extract lung tumor candidates. Conventional maximum intensity projection (MIP) is a technique that projects the three-dimensional volume data with maximum intensity onto a horizontal two-dimensional plane. Here, from the given frame (n), the binarized initial lung segmentation of other frames (n-3, n-2, n-1, n, n+1, n+2, n+3) was projected onto the horizontal two-dimensional plane. The result image on the horizontal two-dimensional plane is used for extracting lung tumor candidates from the ^{18}F-FDG PET images. When optimal lung segmentation is completed in the given frame, the result image is used as the previous frame (n-1) in the AMIP calculation step of the next frame (n+1). AMIP results in two-dimensional images onto which optimal lung segmentation results are repeatedly obtained (Fig. 3).

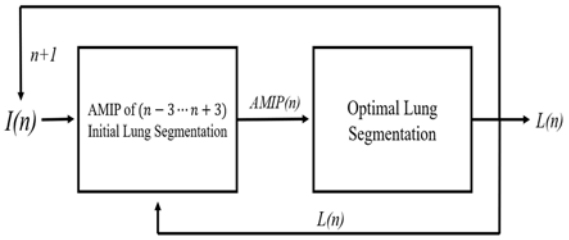


Fig. 3. Diagram of AMIP processing. The diagram is configured as two process blocks. The first block is AMIP processing of initial lung segmentation. The second block is process of optimal lung segmentation. The I(n) is input image, the AMIP(n) is result of AMIP processing in the current frame, and the L(n) is result of optimal lung segmentation. The L(n) is fed back to the first block and the next frame (n+1) is processed. AMIP, adaptive maximum intensity projection; I, input image; L, result of optimal lung segmentation

2.6. Lung Tumor Candidate Extraction from PET/CT Images

Standardized uptake value (SUV) is a value that quantitatively represents the amount of glucose uptake of cancer cells after ^{18}F-FDG distribution in ^{18}F-FDG PET image [11]. In addition, SUV represents the ratio of radioisotope uptake of a tumor tissue to the radioisotope uptake of normal tissues and may be used to distinguish between benign and malignant nodules. It is defined as expression (1).

$$SUV = \frac{\text{radiactivity concentration per gram of tumor } \left(\frac{mCi}{g}\right)}{\text{total injected} \frac{\text{dose}(mCi)}{\text{patientbodyweight}}(g)} \quad (1)$$

Tumors have relatively higher SUVs on ^{18}F-FDG PET images. In this study, we calculated SUVs from ^{18}F-FDG PET images in order to extract lung tumor candidates and used the Otsu algorithm with threshold of 0.75 for binarization of the pixels. However, in addition to tumors, relatively high SUVs were also observed in the liver and heart.

Lung tumor candidates were identified from the binarized SUV results by using jaccard index between the binarized SUV results and AMIP. Here, jaccard index represents the degree to which the binarized SUV results overlap with the AMIP region. Jaccard index values greater than 0.85 were defined as the final lung tumor candidates. The expression for jaccard index calculation is defined as (2).

$$JI = \frac{(AMIP \cap BR)}{BR}, \text{ if } JI \geq 0.85, BR \text{ is Candidate} \quad (2)$$

here, JI is the jaccard index, AMIP is the adaptive maximum intensity projection, and BR is the binarized SUV result value. We compared the AMIP region with the CT and ^{18}F-FDG PET images (Fig. 4).

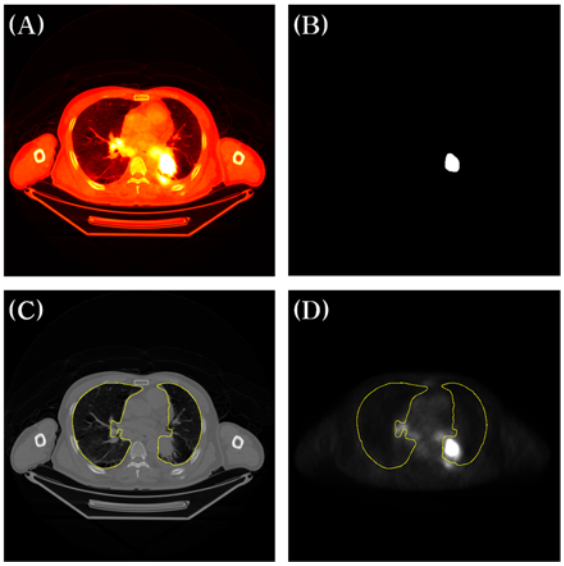


Fig. 4. The comparison results between PET/CT image and AMIP. (A) PET/CT image, (B) Threshold-based tumor candidate extraction, (C) comparison result between CT and AMIP (yellow), (D) comparison result between SUV and AMIP (yellow). PET/CT, ^{18}F-fluorodeoxyglucose integrated positron emission tomography and computed tomography; CT, computed tomography; AMIP, adaptive maximum intensity projection; SUV, standardized uptake value.

The shapes of lung tumor candidates extracted based on the SUV threshold value do not include the anatomical structure characteristics. In order to detect the accurate shape of tumors, the positional information of the lung tumor candidates were set as seed points and seed-based region growing was performed in the AMIP region of the CT images, with 1.5 times the major axis defined as the maximum growing distance from the initial seed points.

2.7. Optimal Lung Segmentation

For accurate segmentation of lung and lung cancer, seed-based region growing algorithm was used. When employing the region growing method, initial seed points, threshold value, and maximum distance from the initial seed points are specified by the user and the regions are grown to adjacent regions depending on those initial criteria. In order to perform region growing automatically, pixel values similar to the lung region in the binarized initial lung segmentation were randomly sampled and coordinates of those pixels were extracted. The extracted coordinates were defined as initial seed points.

When performing region growing on images where tumors are present in the lung, the lung region is incompletely segmented due to the differences in pixel value between the lung region and tumor. In order to overcome this issue, tumors were extracted from the CT images first, and the pixels of the extracted tumors were changed to the values similar to those of the lung region before performing region growing (Fig. 5).

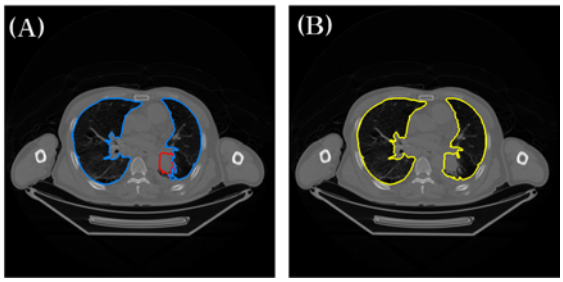


Fig. 5. The result of optimal lung segmentation. (A) Delineation result of tumor segmentation (red) and initial lung segmentation (blue), and the yellow arrow is boundary of two contours. (B) Result of optimal lung segmentation (yellow) using seed-based region growing.

2.8. Algorithm Verification

In this study, we calculated and compared the dice similarity coefficient (DSC), jaccard index, and accuracy (AC) between the segmentation results of the fully automated lung segmentation algorithm and manual analysis in order to assess the performance of the fully automated lung segmentation. Closer the values of DSC, JI, and AC are to 100%, more similar the results of automated lung segmentation and manual lung segmentation. Here, the DSC is defined as expression (3).

$$\mathrm{DSC} = 2\frac{|A \cap M|}{|A|+|M|}, \tag{3}$$

here, A indicates the automated segmentation result, while M indicates the manual segmentation result. In order to calculate the accuracy, a method designed by Udupta, *et al.* was used [11]. Accuracy, true positive (TP), true negative (TN), false positive (FP), and false negative (FN) are defined as expression (4).

$$\begin{aligned} TP &= \frac{|A \cap M|}{|M|} \\ TN &= \frac{|I| - |A \cup M|}{|I| - |M|} \\ FP &= \frac{|M - A|}{|I| - |A|} \\ FN &= \frac{|M - A|}{|M|} \\ Accuracy &= \frac{(TP + TN)}{(TP + FP + TN + FN)} \end{aligned}, \tag{4}$$

here, A indicates the automated segmentation results, B indicates the manual segmentation results, and I indicates the size of the image. In order to assess the performance of the lung tumor extraction result, two experienced nuclear medicine physicians independently interpreted the images, and the manually identified lung tumor positions, which were based on consensus reading of the two physicians, were compared to the positions of tumors extracted by fully automated lung tumor extraction algorithm. For the comparison, the sensitivity, specificity, positive predictive value, negative predictive value, and accuracy of the two approaches were calculated using confusion matrix and were presented in a diagram.

3. Results

In order to develop a fully automated lung segmentation and lung tumor extraction algorithm for PET/CT images, we selected final lung tumor candidates from the initial lung segmentation by comparing AMIP with lung cancer candidates using the jaccard index and extracted lung tumors using seed-based region growing. We successfully developed an optimal lung segmentation and lung tumor extraction algorithm by changing the pixels of the extracted lung tumors to pixel values similar to those of the lung region and performing a seed-based region growing again in the lung region.

We compared the manual lung segmentations of the 264 frames of ^{18}F-FDG PET/CT images obtained from 20 patients with lung cancer with the results of the automated lung segmentation. The comparison showed DSC of 98.2 %, JI of 96.6 %, and AC of 98.8 % (Table 1).

Table 1. Performance of lung segmentation algorithm.

DSC	JI	TP	TN	FP	FN	AC
98.2 (±0.8)	96.6 (±1.5)	97.8 (±1.7)	99.9 (±0.1)	0.08 (±0.1)	2.0 (±1.7)	98.8 (±0.8)
DSC, dice similarity coefficient; JI, jaccard index; TP, true positive; TN, true negative; FP, false positive; FN, false negative; AC, accuracy.						

In order to evaluate the lung tumor extraction performance, the 933 frames of PET/CT images obtained from 20 patients with lung cancer were used for performance comparison analysis. The analysis showed that the fully automated approach had specificity of 89.9 %, sensitivity of 87.9 %, positive predictive value of 75.9 %, negative predictive value of 95.3 %, and accuracy of 88 % (Table 2).

Table 2. Confusion matrix of tumor extraction algorithm.

Prediction				
n=933		**Positive**	**Negative**	**Measure**
Reality	True	250	28	Specificity=88 %
	False	79	576	Sensitivity=90 %
	Mea-sure	PPV=76 %	NPV=95 %	Accuracy=89 %
NPV, negative predictive value; PPV, positive predictive value; n, total frames.				

Fig. 6 sequentially depicts the lung tumor extraction and lung segmentation result of the PET/CT image of an individual.

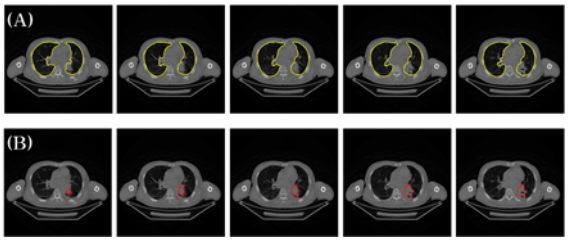


Fig. 6. The result of optimal lung segmentation. (A) Delineation result of tumor segmentation (red) and initial lung segmentation (blue), and the yellow arrow is boundary of two contours. (B) Result of optimal lung segmentation (yellow) using seed-based region growing.

4. Discussion

In this study, we proposed a fully automated lung segmentation and lung tumor extraction algorithm. Traditional lung segmentation approaches had an issue of incomplete lung segmentation due to presence of juxtapleural tumors. This issue was resolved by using ^{18}F-FDG PET images to extract lung tumor candidates and AMIP in CT images. A SUV threshold was used for the ^{18}F-FDG PET images to acquire a binary image, from which lung tumor candidates were extracted. The final lung tumor candidates were selected by calculating jaccard index between the extracted tumor candidates and AMIP results of CT images. The shapes and positions of the lung tumors in the AMIP region of CT images were extracted through seed-based region growing by using the positions of the final lung tumor candidates in the ^{18}F-FDG PET images [13]. The shape of tumors extracted from the CT image were changed into pixel values similar to those of the lung region and seed-based region growing was applied again for the optimal lung segmentation. The accuracy of lung segmentation and lung cancer extraction of this study's fully automated algorithm was 98.8 % and 88.5 %, respectively, demonstrating that this algorithm is highly effective.

PET/CT is of value in differentiating the malignancy and benignity of lung nodule or mass when solitary lung nodule or mass without calcification are observed on chest x-rays or CTs. ^{18}F-FDG PET has a very high sensitivity (97 %) and moderate specificity (78 %) for differential diagnosis of lung nodules or masses [14]. If a patient with lung tumor has a positive PET/CT result, tissue biopsy or pneumonectomy is performed, while patients with negative PET/CT result are clinically followed-up. In the diagnosis process for patients with lung cancer, advanced medical imaging technologies, such as CT, MRI, or PET, have been used historically. However, the medical imaging is becoming increasingly more complex, making it difficult to make accurate diagnosis of patients using the conventional approach. Moreover, physicians' interpretation varied for patients with the same disease depending on the physician's image interpretation skill. With the recent advances in scientific techniques, there have been many attempts of employing computer aided diagnosis for interpreting medical data, such as CT, MRI, and ^{18}F-FDG PET images [15-16]. These CADe and CADx technologies may aid radiologists or nuclear medicine physicians in interpreting CT or ^{18}F-FDG PET images. The use of CADe technology for the diagnosis of PET/CT images of patients with lung cancer not only helps to make accurate diagnosis and decisions of treatment course but also is expected to be of significant socio-economic value.

In order to evaluate the fully automated lung segmentation algorithm, the automated lung segmentation was compared with results obtained by manual lung segmentation from two experienced nuclear medicine physicians. The jaccard index was 96.6 %, dice similarity coefficient was 98.2 %, and accuracy was 98.8 %. The comparison analysis results showed that the jaccard index, dice similarity coefficient, and accuracy were close to 100 %, indicating the results of manual lung segmentation and automated lung segmentation are substantially similar.

The performance of the automated lung cancer extraction algorithm was assessed by comparing a total of 933 frames of PET/CT images with the results of lung tumor positions extracted by two nuclear medicine physicians. The comparison showed that 250 frames were true positives, 28 frames were true negatives, 79 frames were false positives, and 576 frames were false negatives. It is speculated that the main reason for true negatives was that the lung tumor candidates were not accurately extracted during the threshold-based tumor candidate extraction process as the SUV of the lung tumors was relatively too low compared to those of other tissues in the

^{18}F-FDG PET images. The main reason for false positives is thought to be due to the failure of extracting lung tumors accurately from the jaccard index between the AMIP and lung tumor candidates.

A number of studies have been reported that investigated CT image-based segmentation of the lungs with tumors in the lung region or shallowly attached juxtapleural tumors [17-20]. In addition, most of the studies on PET/CT imaging are focused on extraction of lung nodules or tumors using SUVs of ^{18}F-FDG PET images [6, 21]. However, almost no studies have investigated the use of PET/CT images for lung segmentation for cases where large lung tumors, are attached to the pleurae and make it difficult to delineate the boundaries of the lungs. The jaccard index reported in the studies by Wei et al. and Shen et al., which investigated lung segmentation methods that include juxta-pulmonary nodules, was 95.24 % and 97.3 %, respectively. Although the jaccard index of our study (96.6 %) is similar to the two previous studies, our algorithm has strength that it may be used for optimal lung segmentation in cases where large lung tumors are attached to the pleurae.

There are two limitations to this study. First, this study verified data from a small number of patients. Second, as the lung tumor extraction is entirely dependent upon SUVs of PET images, tumors fail to get extracted if SUV is not observed in the corresponding tumors that are detected in the CT image. In future studies, we aim to optimize the algorithm proposed in this study to reduce the false positive rate of lung tumor extraction and apply it to more PET/CT datasets to confirm statistical significance with manual segmentation results.

5. Conclusion

In this study, we developed a fully automated lung segmentation and lung tumor extraction algorithm for PET/CT images. Traditional lung segmentation approaches had an issue of incomplete lung segmentation due to presence of juxtapleural tumors. In order to overcome this issue, we proposed an algorithm that employs the AMIP and seed-based region growing methods. The DSC between the results from the proposed algorithm and manual segmentation was 98.2 %, demonstrating the algorithm is highly effective. We expect this algorithm to aid physicians in interpreting images and making decisions by providing real-time, fully automated interpretation of lung segmentation and lung tumor position.

Acknowledgements

This research is supported by "The Foundation Assist Project of Future Advanced User Convenience Service" through the Ministry of Trade, Industry and Energy (MOTIE) (R0004840, 2018) and Basic Science Research Program through the National Research Foundation of Korea(NRF) funded by the Ministry of Education (NRF-2017R1D1A1B04031182) the Ministry of Trade, Industry and Energy(MOTIE) and Korea Institute for Advancement of Technology(KIAT) through the Research and Development for Regional Industry (R0006452) Korea Health Technology R&D Project through the Korea Health Industry Development Institute (KHIDI), funded by the Ministry of Health & Welfare, Republic of Korea (grant number: HI17C2594).

References

[1]. Jung K.-W., Won Y.-J., Kong H.-J., *et al*., Cancer statistics in Korea: incidence, mortality, survival, and prevalence in 2012, *Cancer Research and Treatment: Official Journal of Korean Cancer Association*, Vol. 47, Issue 2, 2015, pp. 127-141.

[2]. Torre L. A., Bray F., Siegel R. L., Ferlay J., Lortet-Tieulent J., Jemal A., Global cancer statistics, 2012, *CA: A Cancer Journal for Clinicians*, Vol. 65, Issue 2, 2015, pp. 87-108.

[3]. Cerfolio R. J., Ojha B., Bryant A. S., Raghuveer V., Mountz J. M., Bartolucci A. A., The accuracy of integrated PET-CT compared with dedicated PET alone for the staging of patients with nonsmall cell lung cancer, *The Annals of Thoracic Surgery*, Vol. 78, Issue 3, 2004, pp. 1017-1023.

[4]. Bar-Shalom R., Yefremov N., Guralnik L., *et al.*, Clinical performance of PET/CT in evaluation of cancer: additional value for diagnostic imaging and patient management, *Journal of Nuclear Medicine*, Vol. 44, Issue 8, 2003, pp. 1200-1209.

[5]. Spick C., Herrmann K., Czernin J., 18F-FDG PET/CT and PET/MRI perform equally well in cancer: evidence from studies on more than 2,300 patients, *Journal of Nuclear Medicine*, Vol. 57, Issue 3, 2016, pp. 420-430.

[6]. Teramoto A., Adachi H., Tsujimoto M., *et al.*, Automated detection of lung tumors in PET/CT images using active contour filter, *SPIE*, 2015.

[7]. Zhao J., Ji G., Qiang Y., Han X., Pei B., Shi Z., A new method of detecting pulmonary nodules with PET/CT based on an improved watershed algorithm, *PLOS ONE*, Vol. 10, Issue 4, 2015, e0123694.

[8]. Ballangan C., Wang X., Eberl S., Fulham M., Feng D., Automated detection and delineation of lung tumors in PET-CT volumes using a lung atlas and iterative mean-SUV threshold, *SPIE 7259, Medical Imaging*, 2009.

[9]. van Ginneken B., Schaefer-Prokop C., Prokop M., Computer-aided diagnosis: how to move from the laboratory to the clinic, *Radiology*, Vol. 261, Issue 3, 2011, pp. 719-732.

[10]. Mansoor A., Bagci U., Foster B., *et al*., Segmentation and image analysis of abnormal lungs at CT: current approaches, challenges, and future trends, *RadioGraphics*, Vol. 35, Issue 4, 2015, pp. 1056-1076.

[11]. Hickeson M., Yun M., Matthies A., *et al*., Use of a corrected standardized uptake value based on the lesion size on CT permits accurate characterization of lung nodules on FDG-PET, *European Journal of Nuclear Medicine and Molecular Imaging*, Vol. 29, Issue 12, 2002, pp. 1639-1647.

[12]. Udupa J. K., Leblanc V. R., Zhuge Y., *et al*., A framework for evaluating image segmentation algorithm, *Computerized Medical Imaging and Graphics*, Vol. 30, Issue 2, 2006, pp. 75-87.
[13]. Adams R., Bischof L., Seeded region growing, *IEEE Transactions on Pattern Analysis and Machine Intelligence*, Vol. 16, Issue 6, 1994, pp. 641-647.
[14]. Gould M. K., Maclean C. C., Kuschner W. G., Rydzak C. E., Owens D. K., Accuracy of positron emission tomography for diagnosis of pulmonary nodules and mass lesions: a meta-analysis, *JAMA*, Vol. 285, Issue 7, 2001, pp. 914-924.
[15]. Doi K., Computer-aided diagnosis in medical imaging: historical review, current status and future potential, *Computerized Medical Imaging and Graphics*, Vol. 31, Issue 4-5, 2007, pp. 198-211.
[16]. Suzuki K., A review of computer-aided diagnosis in thoracic and colonic imaging, *Quantitative Imaging in Medicine and Surgery*, Vol. 2, Issue 3, 2012, pp. 163-176.
[17]. Soltaninejad S., Cheng I., Basu A., Robust Lung Segmentation combining adaptive Concave Hulls with Active Contours, in *Proceedings of the IEEE International Conference on Systems, Man, and Cybernetics (SMC)*, 2016.
[18]. Wang J., Guo H., Automatic approach for lung segmentation with juxta-pleural nodules from thoracic CT based on contour tracing and correction, *Computational and Mathematical Methods in Medicine*, Vol. 2016, Issue 3, 2016, pp. 1-13.
[19]. Wei Y., Shen G., Li J.-J., A Fully Automatic Method for Lung Parenchyma Segmentation and Repairing, *Journal of Digital Imaging*, Vol. 26, Issue 3, 2013, pp. 483-495.
[20]. Shen S., Bui A. A. T., Cong J., Hsu W., An automated lung segmentation approach using bidirectional chain codes to improve nodule detection accuracy, *Computers in Biology and Medicine*, Vol. 57, 2015, pp. 139-149.
[21]. Teramoto A., Fujita H., Yamamuro O., Tamaki T., Automated detection of pulmonary nodules in PET/CT images: Ensemble false□positive reduction using a convolutional neural network technique, Medical Physics, Vol. 43, Issue 6 Part 1, 2016, pp. 2821-2827.

Published by International Frequency Sensor Association (IFSA) Publishing, S. L., 2019 (http://www.sensorsportal.com).

